Analysis of Axial Field Magnetic Gears with Halbach Arrays

Matthew Johnson, *Student Member, IEEE*, Matthew C. Gardner, and Hamid A. Toliyat, *Fellow, IEEE*

***Abstract*-- Magnetic gears can scale the torque and speed of rotary systems, while avoiding problems associated with transferring torque through physical contact. This work uses 3D finite element analysis to parametrically characterize the performance benefits which can be obtained from applying Halbach magnet arrays to axial field magnetic gears. It is found that Halbach arrays decrease the flux density in the adjacent back iron, allowing the thickness of these yokes to be reduced. Also, using Halbach arrays increases the magnitude of the desired magnetic flux spatial frequencies in the air gaps, increasing torque, and decreases the magnitude of undesired spatial frequencies, decreasing torque ripple. Additionally, the use of Halbach arrays on both rotors increased the torque volumetric torque density for two different design points by 43.6% and 65.7% to 183.9 and 155.8 kN*m/m^3, respectively, and decreased the cogging torque on both rotors.**

***Index Terms*—Axial flux, finite element analysis, Halbach arrays, hermetic isolation, magnetic gear, torque ripple**

I. Introduction

MAGNETIC gears are a technology that has garnered significant attention in recent years [1]-[4] due to their potential to offer a plethora of advantages over mechanical gears. Like their mechanical counterparts, magnetic gears can be used to scale up and down the torque and speed of rotary systems. However, magnetic gears transfer torque through the modulated interaction of magnetic fields rather than through mechanical teeth. This results in the potential for higher reliability, lower acoustic noise, increased efficiency, and physical isolation between shafts.

Magnetic gears have been proposed for several industrial applications. For wind energy generation, magnetic gears can transform the high torque, low speed rotation of the turbine to a low torque, high speed input for the generator, allowing a significantly smaller generator to be used, without the maintenance required for a mechanical gear [2]. Conversely, in traction applications, such as electric vehicles, a magnetic gear can transform the low torque, high speed rotation of a motor into the required high torque, low speed output, enabling a smaller motor and smaller total system volume and mass [3]. Similarly, magnetic gears have been designed for underwater propulsion, where reduced acoustic noise is critically important [4].

Most of the previous work on magnetic gears has focused on the radial field topology shown in Fig. 1(a). However, recently interest has increased in the axial field topology [5]-[7] shown in Fig. 1(b), despite its additional difficulties in construction, because it can easily be used in situations requiring hermetic isolation. Two methods that have been used to increase the torque density of magnetic gear designs are flux-focusing permanent magnet configurations and Halbach arrays. Flux-focusing arrangements have been applied to both radial [8] and axial [6] field topologies, resulting in high torque densities. The use of Halbach magnetic arrays has been applied to radial field magnetic gears to improve torque density and reduce torque ripple [9]-[11]. However, to the authors' knowledge, Halbach arrays have not been applied to axial field magnetic gears. This study employs parametric 3D finite element (FE) simulations to analyze the benefits obtained by incorporating Halbach arrays into axial field magnetic gears.

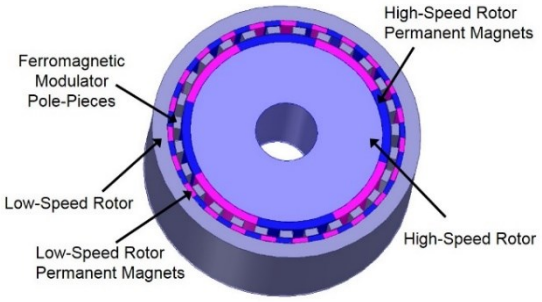

Fig. 1(a). Radial Field Magnetic Gear

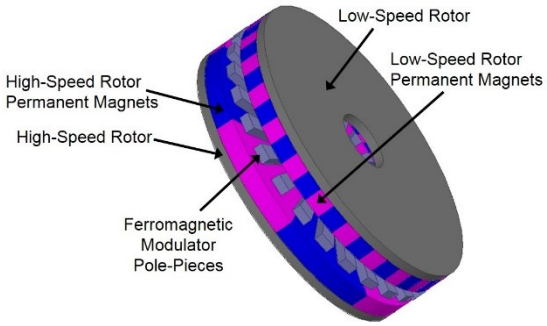

Fig. 1(b). Axial Field Magnetic Gear

M. Johnson, M. C. Gardner, and H. A. Toliyat are with the Advanced Electric Machines and Power Electronics Lab, Texas A&M University, College Station, TX 77843, USA (e-mail: mjohnson11@tamu.edu, gardner1100@tamu.edu, toliyat@tamu.edu).

II. Axial Field Halbach Configurations

The permanent magnet (PM) arrays in a conventional axial field gear consist of magnet pieces with alternating "upward" and "downward" magnetizations, denoted by the blue and purple magnets in Fig. 1(b). Alternatively, an axial Halbach array consists of N_P magnet pieces per pole, with the k^{th} piece having a magnetization angle, γ_k, given by (1) in radians. The individual magnet pieces have both axial and tangential magnetization components which are determined based on γ_k according to (2) and (3). In this manner, a traditional axial field magnetic gear can be viewed as a specific, albeit crude, Halbach configuration with N_P set to 1 for both the high speed rotor (rotor 1) and the low speed rotor (rotor 2) ($N_{P1} = 1$ and $N_{P2} = 1$).

$$\gamma_k = \left(\frac{\pi}{2}\right) \pm \left(\frac{k-1}{N_P}\right) \times \pi \tag{1}$$

$$M_{k,z} = |M| \times \sin(\gamma_k) \tag{2}$$

$$M_{k,\theta} = |M| \times \cos(\gamma_k) \tag{3}$$

A Halbach magnet array, such as the one shown in Fig. 2, creates a more sinusoidal field distribution on one side of the array, while decreasing the field intensity on the other side in a phenomenon known as self-shielding [9]. The "±" sign in (1) is selected as a "+" or a "−" to control the side of the array (top or bottom) on which the field is concentrated. The Halbach array shown in Fig. 2, with $N_P = 3$, produces a pseudo-sinusoidal axial field distribution on its z- side.

Increasing the value of N_P in a Halbach array reduces harmonics in the sinusoidal field distribution on one side while further reducing the field intensity on the other. This can enhance magnetic gear designs by increasing the stall torque, reducing the torque ripple, reducing the requisite amount of back iron material, and improving efficiency. As with traditional (non-Halbach) magnetic gears, the number of pole pairs on rotor 1, P_{PM1}, the number of pole pairs on rotor 2, P_{PM2}, and the number of modulator pieces, Q_M, are still related by (4) resulting in the gear ratio given by (5).

$$Q_M = P_{PM1} + P_{PM2} \tag{4}$$

$$G_r = \frac{\omega_{rotor1}}{\omega_{rotor2}} = \frac{-P_{PM2}}{P_{PM1}} \tag{5}$$

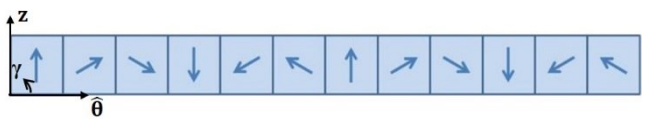

Fig. 2. Halbach Magnet Array (with $N_P = 3$) Focusing the Magnetic Field Below the Array (in the z- Direction)

III. Definition of Key design parameters

A fully parameterized 3D finite element analysis (FEA) model was developed in ANSYS Maxwell to investigate the impact of various design variables on the axial field magnetic gear's performance with and without Halbach arrays. A summary of the most important parameters is provided in Table I. For all design points presented in this study, both air gap thicknesses were fixed at 2 mm and the modulator thickness was held constant at 10 mm.

In an effort to reduce the dimensionality of the parametric design space, three interconnecting design parameters, K_{BI1}, K_{BI2}, and G_r, were each developed to set one design variable as a dependent function of another design variable. Descriptions of these parameters are provided in Table 1 and their mathematical definitions are given in (6) – (8). In particular, the G_r parameter and the associated relationship given by (8) were employed to ensure that all design points used pole pair combinations with relatively large least common multiples (LCMs), which is crucial for achieving low torque ripple performance [2].

TABLE I
Descriptions of Basic Design Parameters

Parameter	Description
P_{PM1}	Rotor 1 magnetic pole pairs
P_{PM2}	Rotor 2 magnetic pole pairs
G_r	Closest integer gear ratio not exceeding the actual gear ratio. Floor(Gear Ratio)
N_{P1}	Rotor 1 magnet pieces per pole
N_{P2}	Rotor 2 magnet pieces per pole
R_1	Axial gear inner radius
R_2	Axial gear outer radius
T_{PM1}	Axial thickness of the rotor 1 magnets
T_{PM2}	Axial thickness of the rotor 2 magnets
T_{AG}	Axial thickness of both air gaps
T_{Mods}	Axial thickness of the modulators
k_{BI1}	Ratio of the rotor 1 back iron and magnet axial thicknesses
k_{BI2}	Ratio of the rotor 2 back iron and magnet axial thicknesses

$$k_{BI1} = \left(\frac{\text{Rotor 1 Back Iron Thickness}}{\text{Rotor 1 Magnet Thickness}}\right) \tag{6}$$

$$k_{BI2} = \left(\frac{\text{Rotor 2 Back Iron Thickness}}{\text{Rotor 2 Magnet Thickness}}\right) \tag{7}$$

$$P_{PM2} = G_r \times P_{PM1} + 1 \tag{8}$$

IV. Back Iron Flux Density Studies

The self-shielding effect of Halbach arrays can be used to significantly decrease the flux density in the magnetic gear's back irons. In turn, this can be used to build a smaller, lighter gear while maintaining performance ratings and even decreasing losses (especially since the arrays also decrease harmonic amplitudes). To quantify this effect, the rotor 1 back iron thickness was held constant while the rotor 1 Habach number (N_{P1}) was swept from 1 to 4 at different rotor 1 pole pair values and the resulting maximum back iron 1 (BI_1) flux densities are depicted in Fig. 3. A similar analysis is shown for rotor 2 in Fig. 4. Both studies were conducted at $G_r = 4$ design points. For each parametric graph presented in this study, the values of pertinent design parameters which were held constant in the corresponding analysis are provided in the graph's caption.

The results in Fig. 3 and Fig. 4 demonstrate that the back iron flux densities can be significantly reduced by the use of Halbach arrays, with the largest improvements observed in the transition from N_P =1 to N_P = 2 on either rotor. As the N_P value is increased beyond 2, the back iron flux densities continue to decrease at a slower rate. Thus, the value of these diminishing returns must be weighed against the increased manufacturing complexity.

Furthermore, a comparison of the data for the two rotors reveals that increasing N_{P1} has a much more profound impact on the rotor 1 back iron flux density than increasing N_{P2} has on the rotor 2 back iron flux density. This is due in part to the fact that rotor 2 already inherently has more pole pairs than rotor 1, in accordance with the gear ratio, and thus has shorter tangential flux paths. The higher pole pair count on rotor 2 also imposes the practical limitation that N_{P2} should be restricted to a smaller range of values than N_{P1} because of manufacturing complexity considerations.

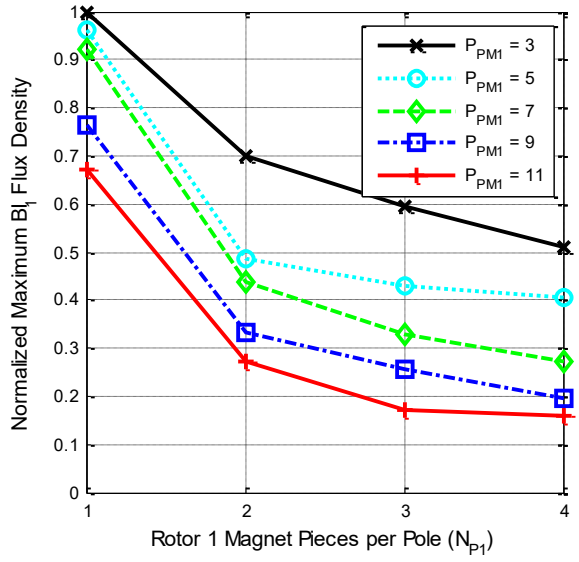

Fig. 3. Rotor 1 Maximum Back Iron Flux Density Variation with Rotor 1 Magnet Pieces per Pole (N_{P1}). Fixed Values: (N_{P2} = 1; k_{BI1} = 1; k_{BI2} = 1; T_{PM1} = 12.7 mm; T_{PM2} = 6.35 mm; R_1 = 100 mm; R_2 = 167 mm; G_r = 4).

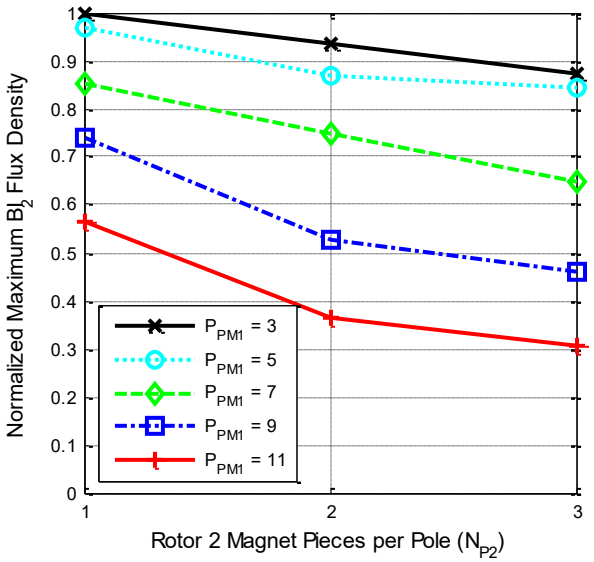

Fig. 4. Rotor 2 Maximum Back Iron Flux Density Variation with Rotor 2 Magnet Pieces per Pole (N_{P2}). Fixed Values: (N_{P1} = 1; k_{BI1} = 1; k_{BI2} = 1; T_{PM1} = 12.7 mm; T_{PM2} = 6.35 mm; R_1 = 100 mm; R_2 = 167 mm; G_r = 4).

The impact of the Halbach arrays on the back iron flux densities was also examined by sweeping the back iron thicknesses at different Halbach numbers with all other design parameters held constant. The results are shown for rotor 1 in Fig. 5 and rotor 2 in Fig. 6. The graph in Fig. 5 reveals that using a Halbach array on rotor 1 can achieve back iron flux density reductions comparable to those obtained by tripling the rotor 1 back iron thickness. The plot in Fig. 6 shows that although the rotor 2 Halbach self-shielding effect is not as significant as seen on rotor 1, it can still result in back iron flux density reductions comparable to those achieved by a 50% increase in the rotor 2 back iron thickness.

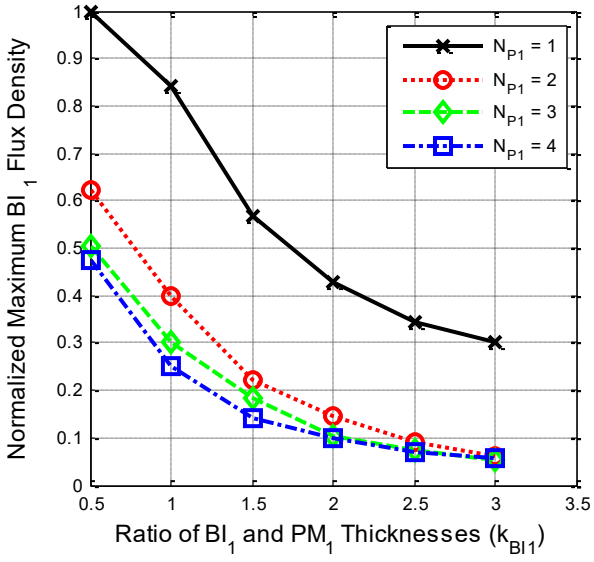

Fig. 5. Rotor 1 Maximum Back Iron Flux Density Variation with Rotor 1 Back Iron Thickness Ratio. Fixed Values: (N_{P2} = 1; P_{PM1} = 7; k_{BI2} = 1; T_{PM1} = 12.7 mm; T_{PM2} = 6.35 mm; R_1 = 100 mm; R_2 = 167 mm; G_r = 4).

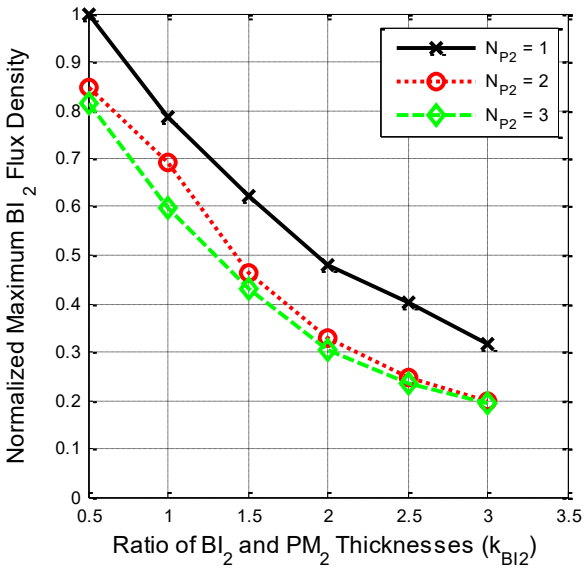

Fig. 6. Rotor 2 Maximum Back Iron Flux Density Variation with Rotor 2 Back Iron Thickness Ratio. Fixed Values: (N_{P1} = 1; P_{PM1} = 7; k_{BI1} = 1; T_{PM1} = 12.7 mm; T_{PM2} = 6.35 mm; R_1 = 100 mm; R_2 = 167 mm; G_r = 4).

V. Air Gap Flux Density Studies

The effects of the Halbach arrays on the air gap axial flux densities were also examined for a 28:3 gear (P_{PM1} = 3, P_{PM2} = 28). Fig. 7 shows an FFT analysis of the axial flux density in the air gap adjacent to rotor 2 with only the rotor 1 magnets and the modulators included in the system. Similarly, Fig. 8 shows an FFT analysis of the axial flux density in the air gap adjacent to rotor 1 with only the rotor 2 magnets and the modulators in the system. These graphs illustrate that the Halbach arrays significantly increase the amplitude of the desired spatial harmonics while also reducing the amplitude of most of the undesired harmonics. This leads to designs with higher stall torque and reduced torque ripple.

VI. Torque Density and Axial Force Studies

In addition to the flux density studies, the Halbach arrays were also evaluated for their effects on the torque ratings of different axial field magnetic gear designs. As with the back iron flux density studies, the impacts of the Halbach arrays on both rotors were evaluated separately. Fig. 9 and Fig. 11 show the impact of the rotor 1 and rotor 2 Halbach arrays on the axial field magnetic gear's volumetric torque density at G_r = 4 design points with different numbers of poles. Fig. 10 and Fig. 12 show the magnitudes of the corresponding axial forces. From these figures, it is evident that increasing the Halbach number on either rotor increases torque density, at the expense of increased axial forces, which necessitate increased structural support. Additionally, these figures show that the effects of increasing the Halbach number decrease at higher values. Due to these diminishing returns, as well as the manufacturing difficulties induced by increasing Halbach numbers, designs with N_{P1} = 3 and N_{P2} = 2 were chosen for further simulation comparison with N_{P1} = 1 and N_{P2} = 1 (non-Halbach array) design points. The Halbach array and non-Halbach array gears were compared at both Gr = 4 and Gr = 9 design points. The other values of the parameters are provided in Table II for G_r values of 4 and 9. The resulting volumetric torque densities are given in Table III. This shows a 43.6% increase in torque density for G_r = 4 and a 65.7% increase in torque density for G_r = 9.

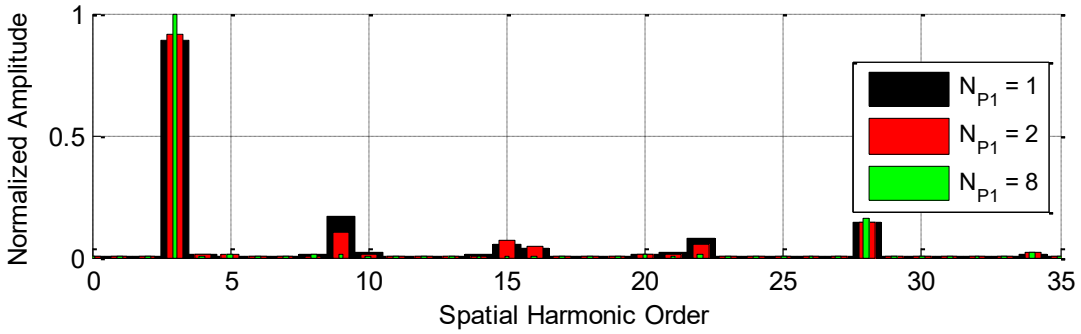

Fig. 7. FFT Analysis of N_{P1} Effects on Rotor 2 Air Gap Axial Flux Density with only Rotor 1 Magnets and Modulators

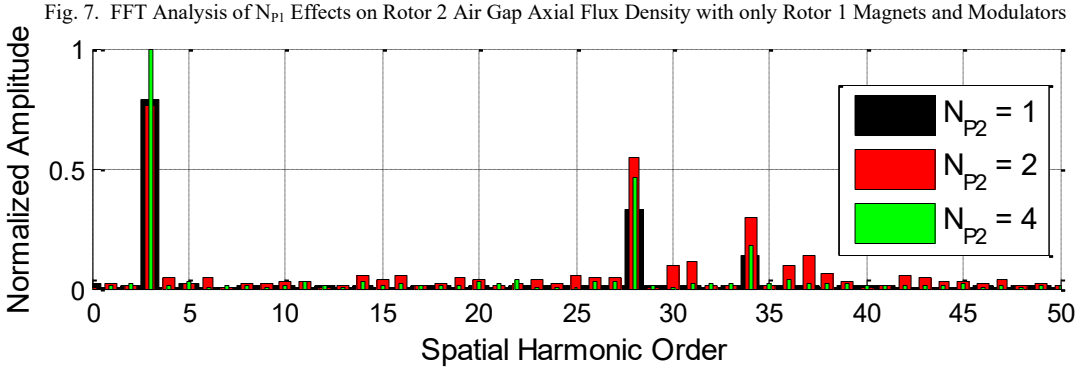

Fig. 8. FFT Analysis of N_{P2} Effects on Rotor 1 Air Gap Axial Flux Density with only Rotor 2 PMs and Modulators

TABLE II
Values of Design Parameters

Parameter	Value for $G_r = 4$	Value for $G_r = 9$
P_{PM1}	7	5
P_{PM2}	29	46
R_1	100 mm	100 mm
R_2	167 mm	167 mm
T_{PM1}	12.7 mm	12.7 mm
T_{PM2}	6.35 mm	6.35 mm
T_{AG}	2 mm	2 mm
T_{Mods}	10 mm	10 mm
k_{BI1}	0.5	0.5
k_{BI2}	0.5	0.5

TABLE III
Volumetric Torque Density Results

Volumetric Torque Density ($kN*m/m^3$)	$N_{P1} = 1$ $N_{P2} = 1$	$N_{P1} = 3$ $N_{P2} = 2$
$G_r = 4$	128.1	183.9
$G_r = 9$	94.0	155.8

Fig. 13 and Fig 14. show the effects of the back iron thicknesses on the torque density for different Halbach numbers. This data demonstrates that increasing N_{P1} and N_{P2} significantly improves volumetric torque density for thin back irons because they become saturated easily, but the self-shielding effect of the Halbach array decreases the flux density passing through the back irons. For higher back iron thicknesses, there is no danger of saturation, which reduces the benefit of increasing the Halbach number. Both figures also indicate that maximum torque density is achieved with no back iron for N_P greater than 1. These air core design points deserve further study, as they offer excellent torque density, but present other difficulties, such as structural support and magnetic containment.

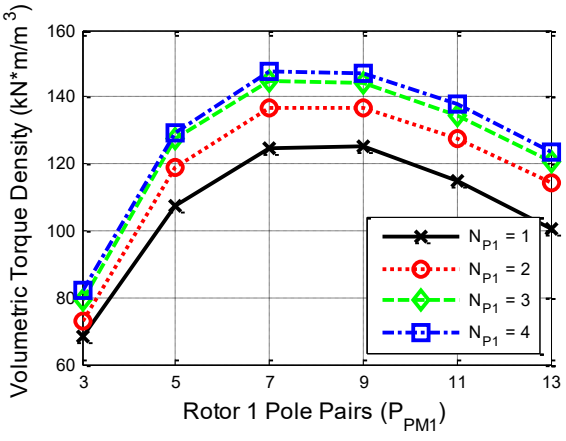

Fig. 9. Volumetric Torque Density Variation with Rotor 1 Pole Pairs for Different Rotor 1 Halbach Configurations at $G_r = 4$. Fixed Values: ($N_{P2} = 1$; $k_{BI1} = 0.5$; $k_{BI2} = 1$; $T_{PM1} = 12.7$ mm; $T_{PM2} = 6.35$ mm; $R_1 = 100$ mm; $R_2 = 167$ mm; $G_r = 4$).

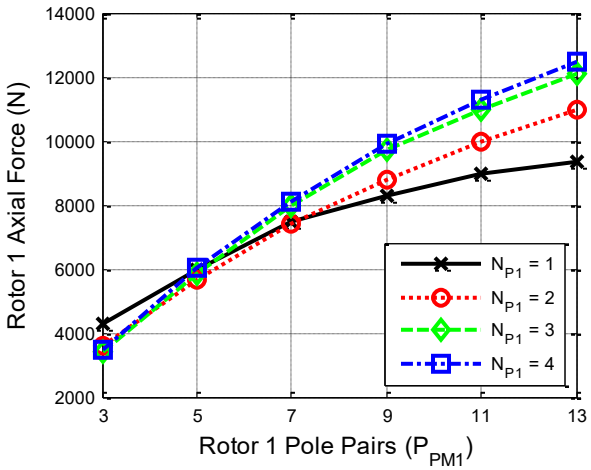

Fig. 10. Impact of Rotor 1 Pole Pairs on Rotor 1 Axial Force for Different Rotor 1 Halbach Configurations at $G_r = 4$. Fixed Values: ($N_{P2} = 1$; $k_{BI1} = 0.5$; $k_{BI2} = 1$; $T_{PM1} = 12.7$ mm; $T_{PM2} = 6.35$ mm; $R_1 = 100$ mm; $R_2 = 167$ mm; $G_r = 4$).

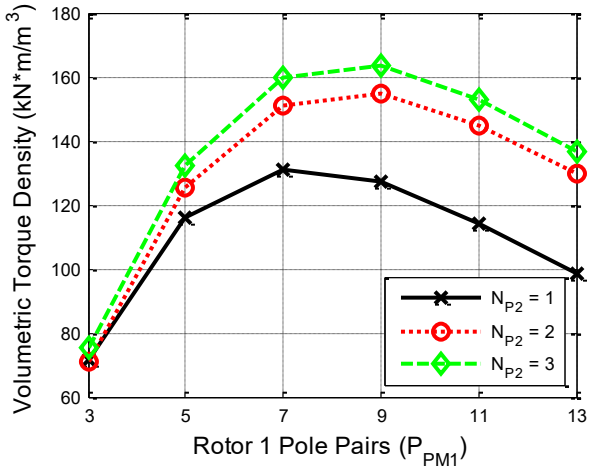

Fig. 11. Volumetric Torque Density Variation with Rotor 1 Pole Pairs for Different Rotor 2 Halbach Configurations at $G_r = 4$. Fixed Values: ($N_{P1} = 1$; $k_{BI1} = 1$; $k_{BI2} = 0.5$; $T_{PM1} = 12.7$ mm; $T_{PM2} = 6.35$ mm; $R_1 = 100$ mm; $R_2 = 167$ mm; $G_r = 4$).

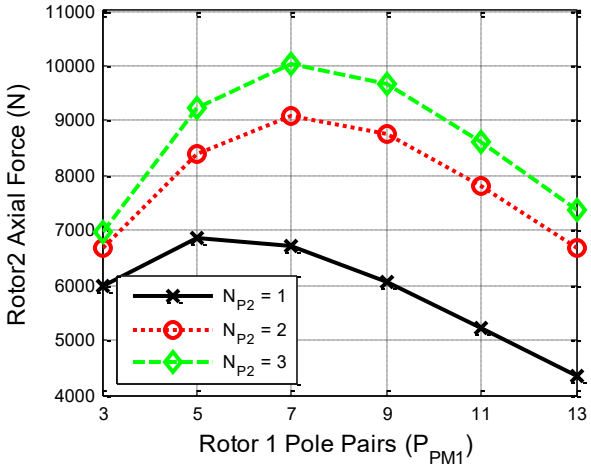

Fig. 12. Impact of Rotor 1 Pole Pairs on Rotor 2 Axial Force for Different Rotor 2 Halbach Configurations at $G_r = 4$. Fixed Values: ($N_{P1} = 1$; $k_{BI1} = 1$; $k_{BI2} = 0.5$; $T_{PM1} = 12.7$ mm; $T_{PM2} = 6.35$ mm; $R_1 = 100$ mm; $R_2 = 167$ mm; $G_r = 4$).

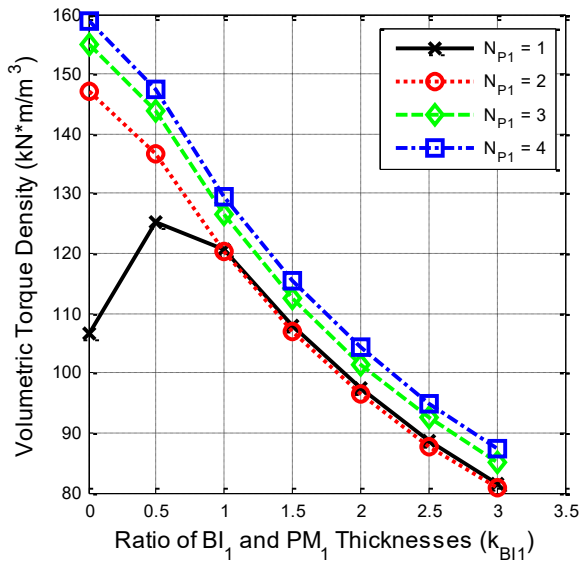

Fig. 13. Volumetric Torque Density Variation with Rotor 1 Back Iron Thickness Ratio. Fixed Values: (N_{P2} = 1; P_{PM1} = 9; k_{BI2} = 1; T_{PM1} = 12.7 mm; T_{PM2} = 6.35 mm; R_1 = 100 mm; R_2 = 167 mm; G_r = 4).

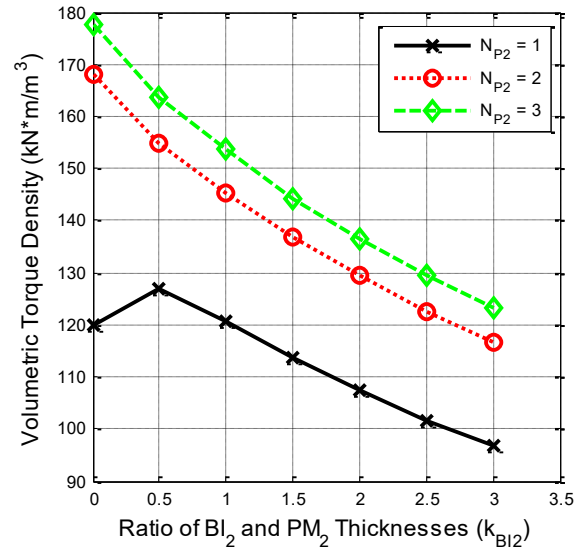

Fig. 14. Volumetric Torque Density Variation with Rotor 2 Back Iron Thickness Ratio. Fixed Values: (N_{P1} = 1; P_{PM1} = 9; k_{BI1} = 1; T_{PM1} = 12.7 mm; T_{PM2} = 6.35 mm; R_1 = 100 mm; R_2 = 167 mm; G_r = 4).

VII. Cogging Torque Studies

The same design points listed in Table II were also evaluated to determine their respective levels of torque ripple at different loads. The results are shown in Fig. 15 for the rotor 1 torque and Fig. 16 for the rotor 2 torque. The load is represented by the electromagnetic torque angle, which describes the relative electromagnetic angular position of the two rotors. An electromagnetic torque angle of 90 degrees corresponds to maximum torque transmission and a torque angle of 0 degrees ideally corresponds to no torque transmission. This data clearly illustrates that the Halbach arrays reduce the torque ripple on both rotors for both gear ratio designs by 50-75%. This reduction in cogging torque is a result of the trends discussed in the air gap flux density study. The Halbach arrays significantly increase the amplitude of the fundamental air gap flux density component relative to the undesirable harmonic air gap flux density components which produce the torque ripple.

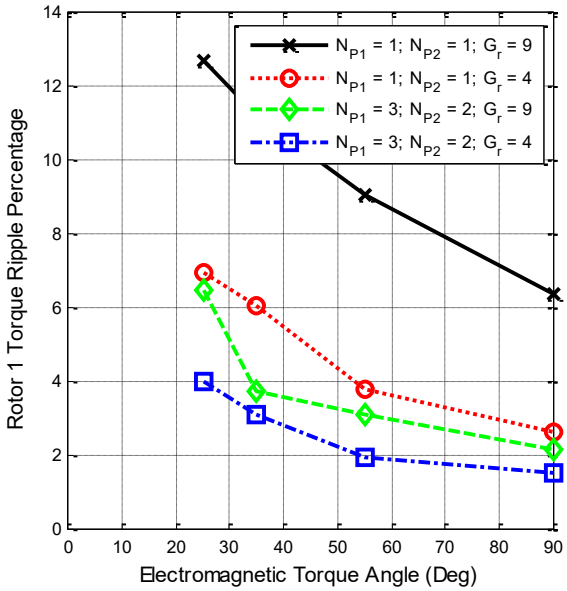

Fig. 15. Variation of Rotor 1 Torque Ripple with Torque Angle for Halbach Array and non-Halbach Array Designs. Fixed Values: (k_{BI1} = 0.5; k_{BI2} = 0.5; T_{PM1} = 12.7 mm; T_{PM2} = 6.35 mm; R_1 = 100 mm; R_2 = 167 mm).

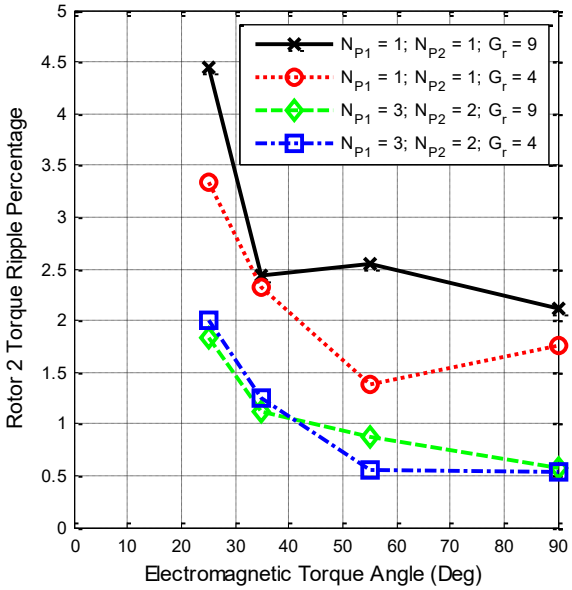

Fig. 16. Variation of Rotor 2 Torque Ripple with Torque Angle for Halbach Array and non-Halbach Array Designs. Fixed Values: (k_{BI1} = 0.5; k_{BI2} = 0.5; T_{PM1} = 12.7 mm; T_{PM2} = 6.35 mm; R_1 = 100 mm; R_2 = 167 mm).

VIII. Conclusion

The arrangement of the permanent magnets into Halbach arrays for an axial field magnetic gear was proposed and analyzed. Parametric FEA simulations were run to analyze trends related to the Halbach numbers and other design parameters of the magnetic gear topology. It was shown that

implementing Halbach arrays decreased the magnetic flux density in the back irons, which can decrease losses and allow for thinner back irons. Additionally, with the implementation of Halbach arrays, the desirable harmonics of the magnetic flux density in the air gaps increased, while the undesirable harmonics decreased. Volumetric torque density and axial forces were shown to increase with Halbach number.

Based on the results of several trends, design points were picked for further simulation. For a gear ratio of 4.14, it was shown that using Halbach arrays on both rotors could elevate the torque density from 128.1 kN*m/m^3 to 183.9 kN*m/m^3, an increase of 43.6%. For a gear ratio of 9.2, using Halbach arrays on both rotors raised the torque from 94.0 kN*m/m^3 to 155.8 kN*m/m^3, an increase of 65.7%. Finally, it was demonstrated that the Halbach arrays lowered the torque ripple on both rotors under several different load conditions. Thus, Halbach arrays can significantly improve the performance of axial field magnetic gears.

IX. Acknowledgment

The authors would like to thank ANSYS for its generous support of the EMPE lab through the provision of FEA software.

X. References

[1] K. Atallah and D. Howe, "A novel high-performance magnetic gear," *IEEE Trans. Magn*., vol. 37, no. 4, pp. 2844–2846, Jul. 2001.

[2] N. Frank and H. Toliyat, "Gearing ratios of a magnetic gear for wind turbines," in *Proc. IEEE Int. Elect. Mach. Drives Conf*., May 3–6, 2009, pp. 1224–1230.

[3] A. Rotondale, M. Villani, and L. Castellini, "Analysis of high-performance magnetic gears for electric vehicle," in *Proc. IEEE Int. Elect. Veh. Conf*., Dec. 17-19, 2014, pp. 1-6.

[4] L. MacNeil, B. Claus, and R. Bachmayer, "Design and evaluation of a magnetically-geared underwater propulsion system for autonomous underwater and surface craft," in *Proc. Int. Conf. IEEE Oceans'14*, St. John's, Canada, Sep. 2014, pp. 1-8.

[5] M. Johnson, A. Shapoury, P. Boghrat, M. Post, and H. Toliyat, "Analysis and development of an axial flux magnetic gear," in *Proc. IEEE Energy Convers. Congr. Expo*, 2014, pp. 5893-5900.

[6] V. Acharya, M. Calvin, and J. Bird, "A low torque ripple flux focusing axial magnetic gear," in *Proc. 7th IET int. Conf. Power Electron., Mach. Drives*, 2014, pp. 1-6.

[7] R.-J. Wang et al., "Design and evaluation of a disc-type magnetically geared PM wind generator," in *Proc. Int. Conf. Power Eng., Energy & Electr. Drives*, 2013, pp.1259-1264.

[8] K. Uppalapati, J. Bird, J. Wright, J. Pitchard, M. Calvin, and W. Williams, "A magnetic gearbox with an active region torque density of 239Nm/L," in *Proc. IEEE Energy Convers. Congr. Expo*, 2014, pp. 1422-1428.

[9] L. Jian and K. Chau, "A Coaxial Magnetic Gear With Halbach Permanent-Magnet Arrays," *IEEE Trans. Energy Conv*., vol. 25, no. 2, pp. 319-328, Jun. 2010.

[10] L. Jing and Y. Zhang, "Exact analytical method for magnetic field computation in the concentric magnetic gear with Halbach permanent-magnet arrays," in *Proc. IEEE Int. Conf. Appl. Superconductivity Electromagnetic Devices*, Oct. 2013, pp. 343-346.

[11] L. Jian, K. Chau, Y. Gong, J. Jiang, C. Yu, and W. Li, "Comparison of coaxial magnetic gears with different topologies," *IEEE Trans. Magn*., vol. 45, no. 10, pp. 4526–4529, Oct. 2009.

XI. Biographies

Matthew Johnson (M' 13) earned his B.S. in electrical engineering from Texas A&M University, College Station, Texas in 2011. During his academic career, he completed multiple internships with L-3 Communications, Raytheon, and Knowledge Based Systems Inc. He is currently pursuing a Ph.D. in electrical engineering while working in the Advanced Electric Machines and Power Electronics Laboratory at Texas A&M University. His research interests include magnetic gears, magnetically geared machines, and motor drives. He has published and presented papers at multiple IEEE conferences and is an IEEE student member.

Matthew C. Gardner earned his B.S. in electrical engineering with a minor in Computer Science from Baylor University, Waco, Texas in 2014. He is currently pursuing a Ph.D. in electrical engineering while working in the Advanced Electric Machines and Power Electronics Laboratory at Texas A&M University.

Hamid A. Toliyat (S'87, M'91, SM'96, F'08) received the B.S, degree from Sharif University of Technology, Tehran, Iran in 1982, the M.S. degree from West Virginia University, Morgantown, WV in 1986, and the Ph.D. degree from University of Wisconsin-Madison, Madison, WI in 1991, all in electrical engineering. Following receipt of the Ph.D. degree, he joined the faculty of Ferdowsi University of Mashhad, Mashhad, Iran as an Assistant Professor of Electrical Engineering. In March 1994 he joined the Department of Electrical and Computer Engineering, Texas A&M University where he is currently Raytheon endowed professor of electrical engineering.

Dr. Toliyat has received the prestigious Nikola Tesla Field Award from IEEE in 2014, the Cyrill Veinott Award in Electromechanical Energy Conversion from the IEEE Power Engineering Society in 2004, Patent and Innovation Award from Texas A&M University System Office of Technology Commercialization's in 2007, TEES Faculty Fellow Award in 2006, Distinguished Teaching Award in 2003, E.D. Brockett Professorship Award in 2002, Eugene Webb Faculty Fellow Award in 2000, and Texas A&M Select Young Investigator Award in 1999. He has also received the Space Act Award from NASA in 1999, and the Schlumberger Foundation Technical Awards in 2001 and 2000.

Dr. Toliyat was an Editor of IEEE Transactions on Energy Conversion. He was Chair of the IEEE-IAS Industrial Power Conversion Systems Department of IEEE-IAS, and is a member of Sigma Xi. He is a fellow of the IEEE, the recipient of the 2008 Industrial Electronics Society Electric Machines Committee Second Best Paper Award as well as the recipient of the IEEE Power Engineering Society Prize Paper Awards in 1996 and 2006 and the 2006 IEEE Industry Applications Society Transactions Third Prize Paper Award. Prof. Toliyat has supervised more than 80 graduate students, post docs and research engineers, published over 425 technical papers, presented more than 80 invited lectures all over the world, and has 16 issued and pending US patents. He is the author of DSP-Based Electromechanical Motion Control, CRC Press, 2003, the co-editor of Handbook of Electric Motors - 2nd Edition, Marcel Dekker, 2004, and the co-author of Electric Machines – Modeling, Condition Monitoring, and Fault Diagnosis, CRC Press, Florida, 2013.

He was the General Chair of the 2005 IEEE International Electric Machines and Drives Conference in San Antonio, Texas. Dr. Toliyat is a Professional Engineer in the State of Texas.